Phosphoinositide-interacting regulator of TRP (PIRT) has opposing effects on human and mouse TRPM8 ion channels

Received for publication, April 19, 2018, and in revised form, April 25, 2018 Published, Papers in Press, May 3, 2018, DOI 10.1074/jbc.RA118.003563

Jacob K. Hilton[‡§¶], **Taraneh Salehpour**[‡§¶], **Nicholas J. Sisco**[‡§¶], **Parthasarathi Rath**[‡§¶], **and Wade D. Van Horn**[‡§¶1]

From the [‡]*School of Molecular Sciences, Arizona State University, Tempe, Arizona 85287, the* [§]*Virginia G. Piper Center for Personalized Diagnostics, Biodesign Institute, Arizona State University, Tempe, Arizona 85281, and* [¶]*The Magnetic Resonance Research Center, Arizona State University, Tempe, Arizona 85287*

Edited by Mike Shipston

Transient receptor potential melastatin 8 (TRPM8) is a cold-sensitive ion channel with diverse physiological roles. TRPM8 activity is modulated by many mechanisms, including an interaction with the small membrane protein phosphoinositide-interacting regulator of TRP (PIRT). Here, using comparative electrophysiology experiments, we identified species-dependent differences between the human and mouse TRPM8–PIRT complexes. We found that human PIRT attenuated human TPRM8 conductance, unlike mouse PIRT, which enhanced mouse TRPM8 conductance. Quantitative Western blot analysis demonstrates that this effect does not arise from decreased trafficking of TRPM8 to the plasma membrane. Chimeric human/mouse TRPM8 channels were generated to probe the molecular basis of the PIRT modulation, and the effect was recapitulated in a pore domain chimera, demonstrating the importance of this region for PIRT-mediated regulation of TRPM8. Moreover, recombinantly expressed and purified human TRPM8 S1–S4 domain (comprising transmembrane helices S1–S4, also known as the sensing domain, ligand-sensing domain, or voltage sensing-like domain) and full-length human PIRT were used to investigate binding between the proteins. NMR experiments, supported by a pulldown assay, indicated that PIRT binds directly and specifically to the TRPM8 S1–S4 domain. Binding became saturated as the S1–S4:PIRT mole ratio approached 1. Our results have uncovered species-specific TRPM8 modulation by PIRT. They provide evidence for a direct interaction between PIRT and the TRPM8 S1–S4 domain with a 1:1 binding stoichiometry, suggesting that a functional tetrameric TRPM8 channel has four PIRT-binding sites.

Transient receptor potential melastatin 8 (TRPM8)[2] is a temperature-sensitive ion channel that activates at temperatures below 25 °C; it is considered the primary cold sensor in mammals (1, 2). Besides temperature, TRPM8 activity is modulated by a variety of stimuli, including small molecules (the most well-known of which is menthol), pH, and the phospholipid phosphoinositide 4,5-bisphosphate (PIP_2) (3, 4). Although TRPM8 function is typically considered in the context of sensory physiology, TRPM8 also has important roles in other physiological processes such as pain (5), core body temperature regulation (6–8), body weight regulation (9), vasoconstriction regulation (10), and osmolality sensing (11). Understanding the regulation of TRP channel activity, including TRPM8, is currently an area of much investigation and debate.

TPRM8 activity is also modulated by a phosphoinositide-interacting regulator of TRP (PIRT), a small two-span membrane protein (12, 13). PIRT was originally identified as a regulator of TRPV1, and it is exclusively expressed in dorsal root ganglia, trigeminal ganglia, and enteric neurons of the peripheral nervous system (14). PIRT knockout mice exhibit impaired temperature response to both hot and cold temperatures, and electrophysiology and calcium imaging studies demonstrated that both TRPM8 and TRPV1 activity are enhanced in the presence of PIRT (12, 14). In addition, PIRT was shown to contribute to visceral pain sensation (15), bladder activity regulation (16), and TRPV1-dependent and -independent itch (pruritus) sensation (17), suggesting broader physiological roles and underscoring the biological importance of this modulatory protein. Coimmunoprecipitation experiments show that PIRT interacts with TRPV1 and TRPM8, suggesting that the regulation is mediated via a direct interaction with the channel (14). Cell-surface trafficking experiments indicate that enhanced channel activity in mice is not caused by changes in expression levels or channel trafficking, supporting the idea that PIRT enhances channel activity by interacting directly with the channels rather than increasing the number of channels in the membrane (12, 14). More recently, it was shown that PIRT works synergistically with PIP_2 to enhance TRPM8 currents by increasing conductance at the single channel level (13). However, the details of this interaction including the binding site and stoichiometry of PIRT to TRPM8 are unknown.

Notably, these studies were carried out using mouse models and apparently heterologous expression of the mouse *Pirt* and

This work was supported by a Bisgrove Early Career Award from the Science Foundation Arizona and National Institutes of Health Grant R01GM112077 (to W. V. H.). The authors declare that they have no conflicts of interest with the contents of this article. The content is solely the responsibility of the authors and does not necessarily represent the official views of the National Institutes of Health.

[1] To whom correspondence should be addressed: School of Molecular Sciences, The Biodesign Institute, The Virginia G. Piper Center for Personalized Diagnostics, The Magnetic Resonance Research Center, P. O. Box 871604, Tempe, AZ 85281. Tel.: 480-965-8322; Fax: 480-965-2747; E-mail: wade.van.horn@asu.edu.

[2] The abbreviations used are: TRPM8, transient receptor potential melastatin 8; PIP_2, phospholipid phosphoinositide 4,5-bisphosphate; PIRT, phosphoinositide-interacting regulator of TRP; Ni-NTA, nickel-nitrilotriacetic acid; VSD, voltage-sensing domain; IRES, internal ribosome entry site; HA, hemagglutinin; DPC, dodecylphosphocholine; TROSY, transverse relaxation-optimized spectroscopy; HSQC, heteronuclear single quantum coherence.

Trp channel genes. TRP channels exhibit remarkable functional and sequence diversity not only between different channels in the family, but also between orthologs, *i.e.* the same gene product from different species (18, 19). These differences can manifest as important selected features between species; for example, the thermosensitivity of different species of TRPM8 is evolutionarily tuned to the appropriate temperature range based on organismal core body temperature and environment (20), and avian TRPV1 is insensitive to capsaicin, a potent agonist of the mammalian ortholog, which allows for seed dispersement (19).

The results of this study focus on the human TRPM8 and PIRT gene products and for the first time reveal that in contrast to the increased conductance seen in the mouse proteins, human TRPM8 currents are attenuated in the presence of human PIRT. Analogous to previously published mouse studies, human PIRT does not reduce human TRPM8 cell-surface expression. Additionally, nuclear magnetic resonance (NMR) chemical shift perturbation and *in vitro* pulldown experiments show that PIRT binds specifically to the S1–S4 domain of TRPM8, with a 1:1 stoichiometry. Transmembrane domain chimeras of human/mouse TRPM8 show that residues in the transmembrane domain (helices S1–S6), and in particular the pore domain (S5–S6), are the basis for modulation by PIRT and the species differences observed. These results shed light on the PIRT–TRPM8 interaction and reveal that the PIRT–TRPM8 complex has evolved in a species-dependent manner.

Results

PIRT modulation of TRPM8 is species-dependent

Whole-cell patch clamp electrophysiology was used to measure current responses of human embryonic kidney (HEK) 293 cells that were transiently transfected with either human *TRPM8* and human *PIRT* or human *TRPM8* and empty vector (Fig. 1*A*). Current responses to voltage steps from −100 to +100 mV were recorded using a standard step protocol (Fig. 1*D*). At ambient room temperature (~23 °C), recordings of cells transfected with both human *TRPM8* and *PIRT* resulted in significantly reduced currents compared with cells transfected with human *TRPM8* and an empty pIRES2–DsRed vector at voltages of +60 mV and above; at +100 mV, cells transfected with human *PIRT* showed on average ~69% of the current measured from cells expressing hTRPM8 alone.

We further tested hPIRT modulation of hTRPM8 in the more physiologically relevant context of low temperature and menthol stimuli. In the presence of a TRPM8 saturating concentration of menthol (500 μM) (21), current from human *PIRT*-transfected cells was significantly reduced at and above +30 mV, with ~65% of the maximum current observed at +100 mV (Fig. 1*B*). At 15 °C, a TRPM8 saturating temperature, human *PIRT*-transfected cells exhibited significantly attenuated currents at all measured voltages except −90 mV. At +100 mV, cells expressing hPIRT exhibited ~54% of the current evoked from TRPM8 alone (Fig. 1*C*). Temperature-dependent inward hTRPM8 currents were significantly reduced at physiological voltages (Fig. 1*C*). Statistical significance was determined by an unpaired Student's *t* test; a minimum of 15 and maximum of 43 cells were measured for these conditions and clearly specified in Fig. 1.

Mouse PIRT (mPIRT) has previously been established as an endogenous regulator of TRPM8 that enhances TRPM8 currents (12). Using whole-cell patch clamp experiments, we were able to reproduce these results using the mouse orthologs, with mTPRM8 currents significantly higher in the presence of mPIRT. We note that the hTRPM8 currents are about twice the magnitude of mTRPM8 currents when PIRT was not expressed, highlighting the inherent functional differences between the two TRPM8 orthologs (Fig. 2*A*). Cross-species expression of PIRT with TRPM8 (*e.g.* hTRPM8/mPIRT) did not result in significant differences in currents (Fig. 2*B*).

Previous studies have shown that TRP channel activity can be modulated by associated proteins that regulate channel trafficking to the membrane (22). To test whether hPIRT affects hTRPM8 trafficking, we performed cell-surface expression experiments on HEK-293 cells transfected with human *TRPM8* alone or with human *TRPM8* and *PIRT*. Western blotting quantification from three independent experiments showed no significant difference in hTRPM8 plasma membrane expression levels in the presence and absence of hPIRT expression, confirming that hPIRT does not affect hTRPM8 membrane trafficking (Fig. 3*A*). This agrees with previous similar studies of the mouse orthologs, which show that mouse TRPM8 membrane trafficking is also not affected by mouse PIRT coexpression and that mouse PIRT increases single channel conductance (12–14).

PIRT interacts directly with the TRPM8 S1–S4 domain

Previously reported co-immunoprecipitation studies indicate that mTRPM8 and mPIRT interact in the context of HEK-293 cells (12). In particular, the C-terminal 26 residues of PIRT were shown to bind to both TRPV1 and TRPM8; additionally, a glutathione *S*-transferase-tagged form of the PIRT C terminus was shown to modulate currents from these two channels (12, 14). However, a follow-up study using mTRPV1 and mPIRT fused to fluorescent proteins detected no FRET signal (23). To date, nothing has been published regarding which regions of TRPV1 or TRPM8 interact with PIRT. To further probe the molecular basis of the TRPM8–PIRT complex, we performed an *in vitro* pulldown experiment. Given that PIRT is a small transmembrane protein, we reasoned that it likely interacts with a transmembrane region within TRPM8. TRP channels have a transmembrane topology similar to voltage-gated potassium channels, with six transmembrane helices that form an S1–S4 domain and a pore domain (S5–S6 helices) (18). Using purified hPIRT and hTRPM8 S1–S4 domains, where only the hPIRT protein contained a histidine affinity tag, the two proteins were mixed, bound to Ni-NTA resin, washed extensively (>50 column volumes) and eluted from the column. Analysis of the eluted fractions by SDS-PAGE showed that both hPIRT and hTRPM8 S1–S4 domains were eluted from the mixture, demonstrating that hPIRT interacts directly with the hTRPM8 S1–S4 domain as shown in Fig. 3*B*. The pulldown experiment was performed twice and

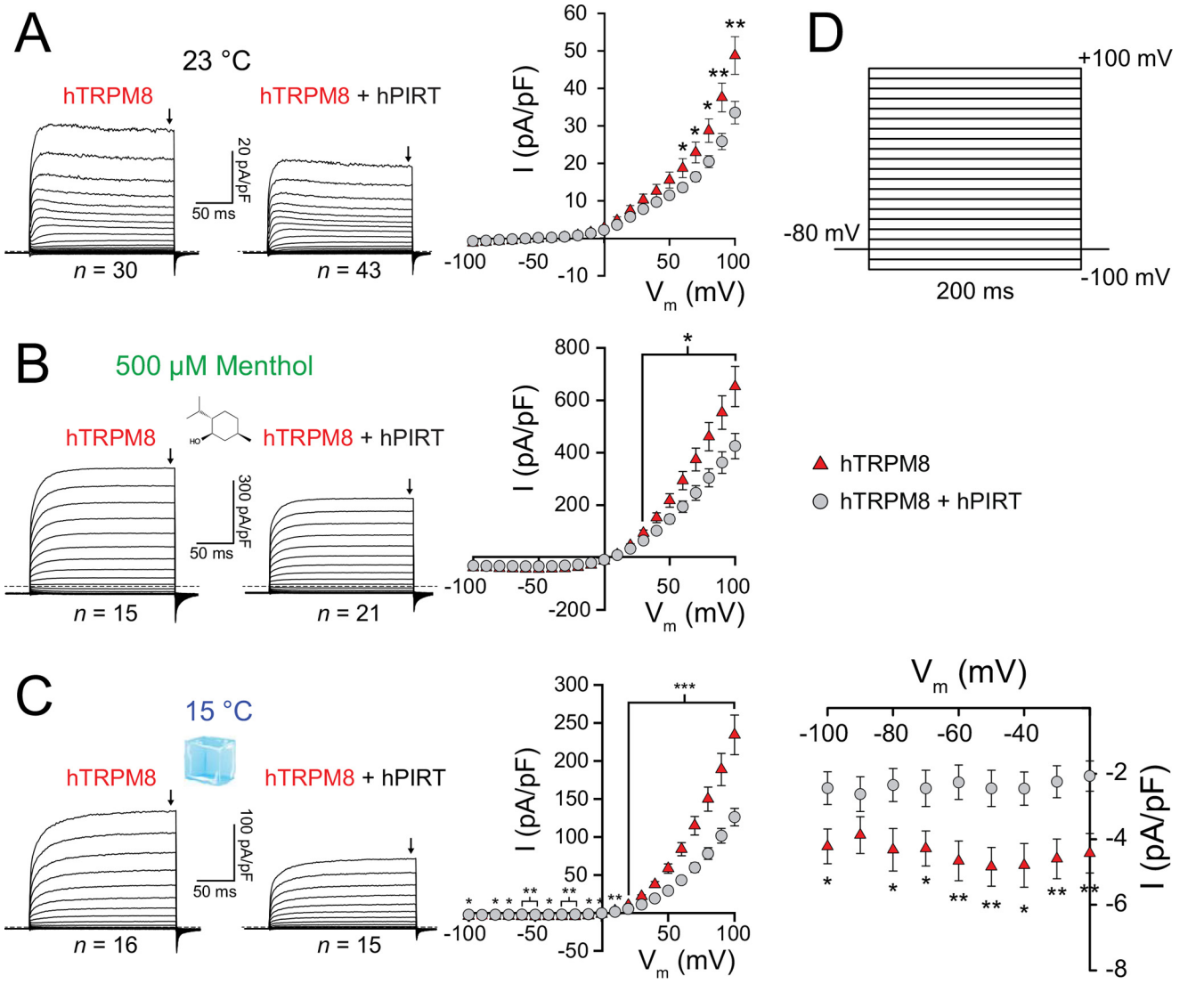

Figure 1. Human PIRT attenuates whole-cell currents of human TRPM8. *A,* average current traces and current-voltage plot of whole-cell patch clamp electrophysiology recordings of HEK-293 cells expressing hTRPM8 or hTRPM8 and hPIRT taken at ambient temperature (23 ± 1 °C). Current-voltage plots are of steady-state current values taken from the time point indicated by an *arrow* in the average current traces. At ambient temperature, hTRPM8 currents are significantly attenuated at voltages above +60 mV when coexpressed with hPIRT. *B,* upon stimulation with saturating menthol concentrations (500 μM), hTRPM8 currents are significantly attenuated at voltages above +30 mV. *C,* cold-evoked currents were significantly attenuated at all measured voltages with the exception of −90 mV. An expanded view of negative potentials (*bottom right*) shows that hPIRT significantly attenuates cold-evoked currents at physiological membrane potentials. *D,* the voltage step protocol used to record current responses from −100 to +100 mV in 10 mV steps with a holding potential of −80 mV between steps. Statistical significance was determined using a two-tailed Student's *t* test; *single asterisk* indicates $p < 0.5$, *double asterisk* indicates $p < 0.01$. *Red triangles* represent cells transfected with human *TRPM8* and empty control vector DNA; *gray circles* represent cells transfected with human *TRPM8* and *PIRT* DNA. *Error bars* represent mean ± S.E.

had consistent results in showing the hTRPM8 S1–S4 domain–PIRT interaction.

To further study this interaction, we performed an NMR titration of ^{15}N-labeled hPIRT with hTRPM8 S1–S4 domain. We used ^{1}H,^{15}N-TROSY-HSQC experiments to measure ^{1}H and ^{15}N chemical shifts of hPIRT with increasing concentrations of the hTRPM8 S1–S4 domain (Fig. 4, *A* and *C*). A number of hPIRT resonances exhibited significant chemical shift perturbation (Δδ) with increasing hTRPM8 S1–S4 domain concentrations. Fig. 4 highlights two representative resonances (Fig. 4*B*) and plots the change in chemical shift (Δδ) as a function of the hTRPM8 S1–S4:hPIRT mole ratio (Fig. 4*D*). Fitting a single binding site model to these plots shows that binding becomes saturated as the molar ratio approaches 1 (Fig. 4*D*). The saturating chemical shift changes of these resonances indicate that the perturbation is the result of direct and specific binding interactions. The calculated K_d values for the two highlighted resonances were near a molar ratio of ~0.5. As a negative control, we expressed and purified the voltage-sensing domain of KCNQ1 (KCNQ1–VSD), a voltage-gated potassium channel that is structurally homologous to TRPM8 but has not been shown to be modulated by PIRT. The TROSY-HSQC titration data of hPIRT and KCNQ1–VSD (Fig. 4, *E* and *F*) indicates that hPIRT does not bind to KCNQ1 as there is nonsaturating and minimal chemical shift perturbation identified in this control experiment. These data confirm the pulldown experimental results and show that hPIRT binds specifically and directly to the hTRPM8 S1–S4 domain with a 1:1 binding stoichiometry.

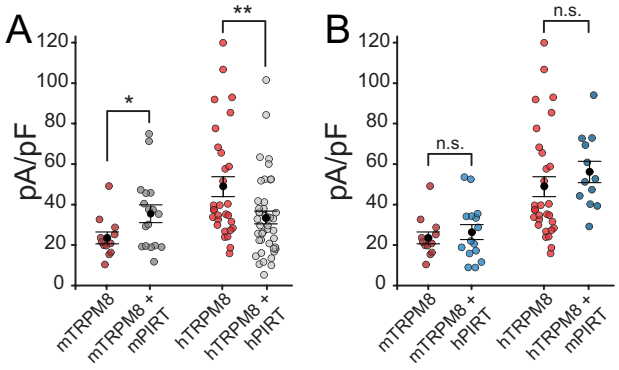

Figure 2. Human and mouse species-dependent PIRT regulation of TRPM8 orthologs. *A,* comparison of steady-state current density measured at room temperature (23 ± 1 °C) from HEK-293 cells coexpressing either mouse or human TRPM8 and PIRT. The presence of mouse PIRT increases current compared with TRPM8 alone, whereas human PIRT has an opposite, attenuating effect. *B,* comparison of TRPM8 currents in the presence and absence of PIRT from the opposite species. No significant difference can be detected between the two conditions. This is likely the result of an intermediate effect. Currents were measured at +100 mV at the same steady-state time point indicated in Fig. 1. (mTRPM8, $n = 12$; mTRPM8 + mPIRT, $n = 17$; mTRPM8 + hPIRT, $n = 15$; hTRPM8, $n = 30$; hTRPM8 + hPIRT, $n = 43$; hTRPM8 + mPIRT, $n = 12$.)

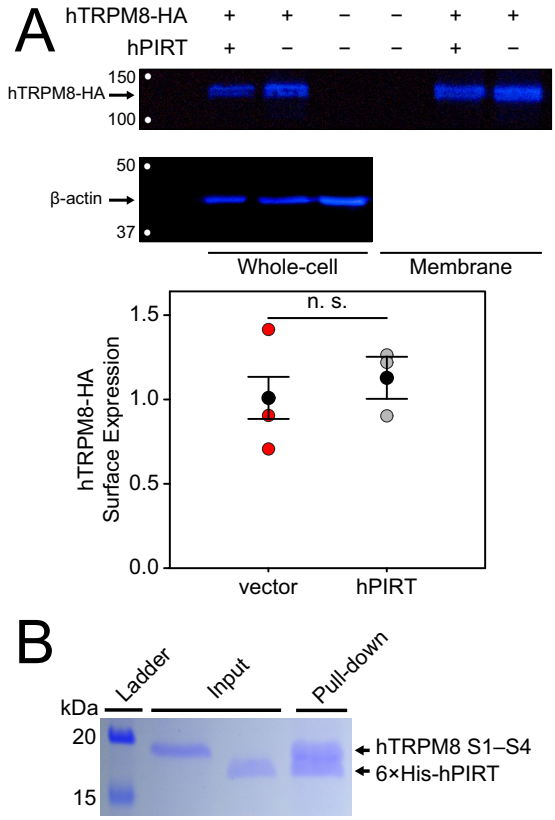

Figure 3. Human TRPM8 cell-surface trafficking is not affected by PIRT expression, and the purified proteins directly interact under *in vitro* conditions. *A,* representative Western blot from trafficking experiments. hTRPM8 cell-surface expression was measured by biotinylation and purification of surface proteins followed by Western blotting. Negative signs indicate conditions in which cells were transfected with empty vector. The *blot* shows similar surface expression levels in the presence and absence of hPIRT. Three experiments were repeated using independently transfected cells, and the results are presented in the scatter plot. *Black circles* represent average expression level, and *error bars* represent mean ± S.E. *B,* human PIRT directly binds the TRPM8 S1–S4 domain. His_6–hPIRT was mixed with the tag-cleaved hTRPM8 S1–S4 domain and the complex was bound to a Ni-NTA column. Coomassie-stained SDS-PAGE revealed that hTRPM8 S1–S4 domain coelutes with PIRT, indicating that the two proteins bind directly.

Functional determinants of PIRT modulation in the TRPM8 transmembrane domain

Chimeric ion channels have proven a valuable research tool for identifying molecular bases of channel regulatory mechanisms and of functional differences between orthologues (19, 24–26). To probe the functional determinants of TRPM8 modulation by PIRT, we generated a series of mouse and human TRPM8 chimeras to search for regions that give rise to species-specific phenotypes. The transmembrane core is known to be the nexus of TRP channel integration of stimuli. Because of this and the concise nature of PIRT, we chose to focus our search on this region, and we generated a series of transmembrane domain (TMD) chimeras. Based on sequence homology with other TRP channels for which cryo-EM structures have been solved, we defined the TMD as residues 672–1012. Within this region, there are only 11 residues that are different between mouse and human TRPM8. A recently determined cryo-EM structure of *Ficedula albicollis* TRPM8 allowed us to map these residues to specific regions in the channel (Fig. 5*A*) (27). Two divergent residues are found in the helical pre-S1 domain, four in the S2 helix, three in the pore loop, one in the S6 helix, and one in the TRP helix. We mutated residues in mTRPM8 to the corresponding residues found in hTRPM8 to generate three chimeric channels: $mTRPM8_{hTMD}$, which includes all 11 residues from hTRPM8; $mTRPM8_{hS1S4}$, which includes only hTRPM8 residues from the S1–S4 domain; and $mTRPM8_{hPD}$, which includes hTRPM8 residues from the pore domain and TRP helix (Fig. 5*B*). We performed electrophysiology measurements to determine whether these chimeras reproduce the human phenotype in the presence of human PIRT.

The $mTRPM8_{hTMD}$ construct produced a phenotype similar to hTRPM8 in the presence of hPIRT. When coexpressed with hPIRT, the channel exhibited 67 ± 13% of the current density without hPIRT at +100 mV with 500 μM menthol; this is close to the reduction observed with WT hTRPM8 and hPIRT (vector only, $n = 15$; hPIRT, $n = 15$; $p = 0.03$). This channel exhibited no difference in current when expressed with or without mPIRT, suggesting that the TMD plays a key role in the modulatory effect (Fig. 5*C*). The $mTRPM8_{hS1S4}$ channel also exhibited a decreased average current density to 67 ± 13% of the current without hPIRT; however, a Student's *t* test resulted in a higher *p* value (vector only, $n = 14$; hPIRT, $n = 14$; $p = 0.1$) (Fig. 5*C*). Finally, $mTRPM8_{hPD}$ showed significantly decreased current density to 75 ± 10% of the current without hPIRT (vector only, $n = 12$; hPIRT, $n = 13$; $p = 0.03$) (Fig. 5*C*). Taken together, these results point to the transmembrane domain, and particularly the pore domain, as key functional determinants of TRPM8 modulation by PIRT.

Intriguingly, the $mTRPM8_{hPD}$ chimera showed significantly increased currents compared with the other chimeras (Fig. 5*D*). An analysis of variance test showed a significant difference between the three groups ($p = 0.0001$; $F = 11.4121$) and a Tukey HSD test showed a significant difference between $mM8_{hPD}$ and $mM8_{hS1S4}$ ($p = 0.004$), and between $mM8_{hPD}$ and $mM8_{hTMD}$ ($p = 0.0002$), but not between $mM8_{hS1S4}$ and

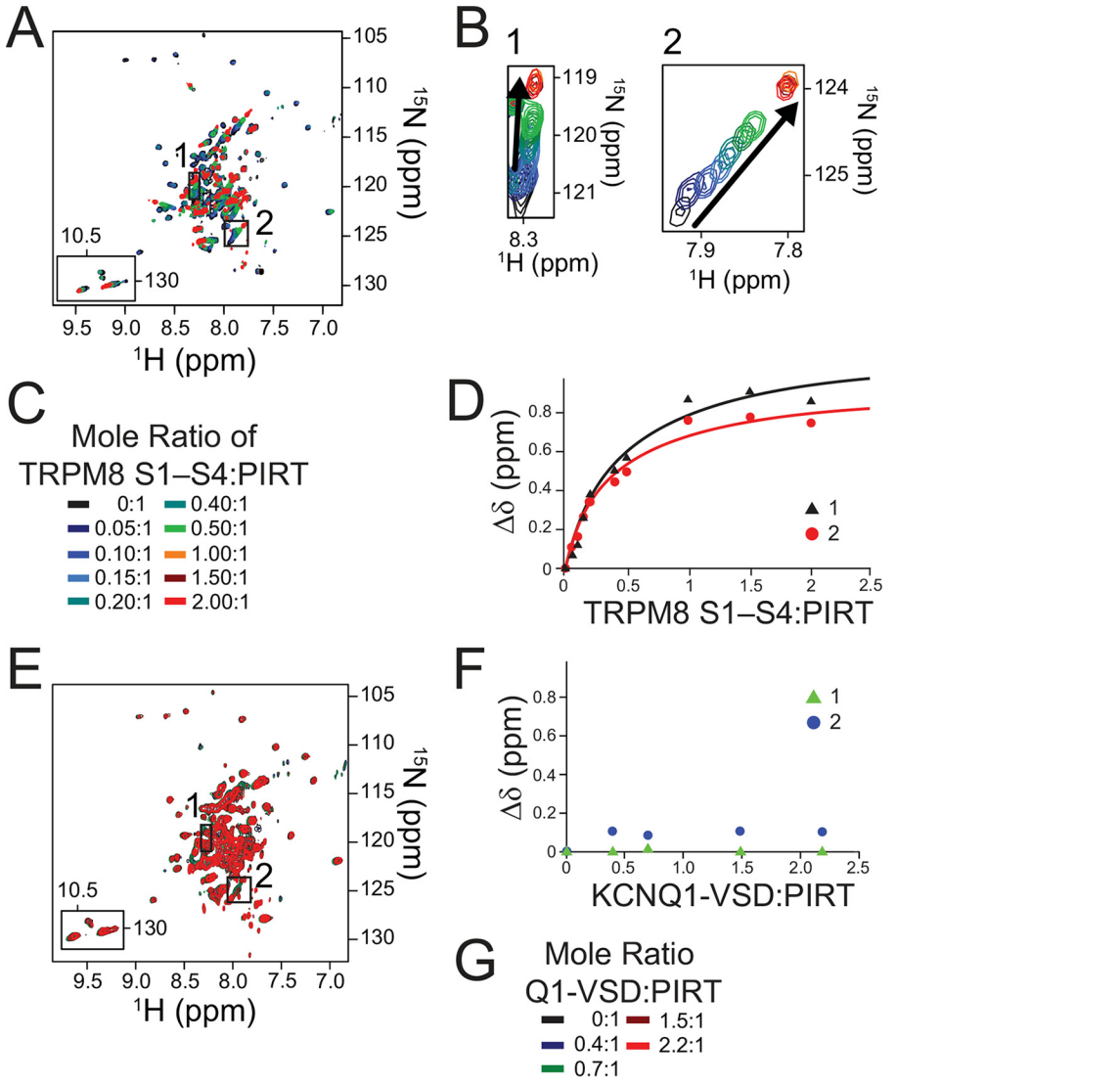

Figure 4. NMR studies show that human PIRT directly binds to the TRPM8 S1–S4 domain. Titration of ^{15}N-labeled hPIRT with unlabeled hTRPM8 S1–S4 domain was performed. *A,* overlaid ^{1}H,^{15}N-TROSY-HSQC spectra from samples with varying hTRPM8 S1–S4 domain:hPIRT mole ratios from 0 to 2. Individual amino acid resonance chemical shift perturbations are highlighted by boxes *1* and *2*. The chemical shifts of these resonances show evidence of saturable binding at elevated TRPM8 S1–S4 domain concentrations. *B,* expanded view of the chemical shift perturbations highlighted in *A*; note that in box 2 of *B* the spectral contours are raised such that the resonances are more easily observed. *C,* the mole ratio legend for the titration of hPIRT with hTRPM8 S1–S4 domain. *D,* normalized change in chemical shift (Δδ) values from both resonances were plotted as a function of hTRPM8 S1–S4 domain:hPIRT mole ratio. The data were fit to a single binding site model using the equation: $f((\Delta\delta) = (\Delta\delta)(\Delta\delta_{max})/K_d + \Delta\delta)$. K_d values for resonances 1 and 2 were calculated to be 0.50 ± 0.11 and 0.41 ± 0.07, respectively, both with r^2 coefficients of 0.98. *E,* overlaid ^{1}H,^{15}N-TROSY-HSQC spectra from samples with varying concentrations of the KCNQ1–VSD. The lack of PIRT chemical shift perturbation upon addition of the KCNQ1–VSD suggests that it does not interact with PIRT. *F,* an equivalent Δδ plot for KCNQ1–VSD:PIRT showing that there is no significant chemical shift perturbation to the corresponding PIRT resonances from *A* upon addition of KCNQ1–VSD to PIRT. *G,* concentration legend for the PIRT–KCNQ1–VSD titration.

mM8$_{hTMD}$ (p = 0.6). WT mTRPM8 current density was also significantly lower compared with WT hTRPM8; thus, the five mutations in the pore domain and TRP helix are sufficient to confer higher, human-like current density to the mTRPM8 chimera.

Discussion

PIRT has previously been shown in behavioral knock-out mice studies to be important in thermosensation via regulation of the thermosensitive TRP channels TRPV1 and TRPM8, demonstrating that the biophysical effects of PIRT on TRPM8 are functionally significant at the organismal level (12, 14). These studies focused on mouse orthologs of both the *Trp* channel and *Pirt* genes. Here, we present data from the human orthologs and show that the human PIRT–TRPM8 interaction results in an opposite modulatory effect compared with the mouse proteins.

Previous studies have investigated PIRT binding with TRP channels. Dong and co-workers (14) expressed the first 53 residues of the N terminus and the last 26 residues of the C terminus fused to glutathione *S*-transferase tags and performed a pulldown assay with mouse TRPV1 and TRPM8. Their results indicate that the PIRT C and N termini bind strongly and weakly to the two TRP channels, respectively (14). However, as whole cell lysate was used, these data do not rule out an indirect interaction with other partner proteins in the complex. A sec-

A

	Residue	Human	Mouse	Location
$mTRPM8_{hTMD}$ / $mTRPM8_{hS1S4}$	709	Phe	Leu	Pre-S1
	717	Val	Ile	Pre-S1
	766	Pro	Thr	S2
	770	Val	Ile	S2
	773	Ser	Ala	S2
	788	Val	Met	S2
$mTRPM8_{hPD}$	921	Gly	Ser	Pore loop
	927	Ala	Ser	Pore loop
	932	Thr	Ser	Pore loop
	985	Thr	Ile	S6
	1007	Ser	Asn	TRP helix

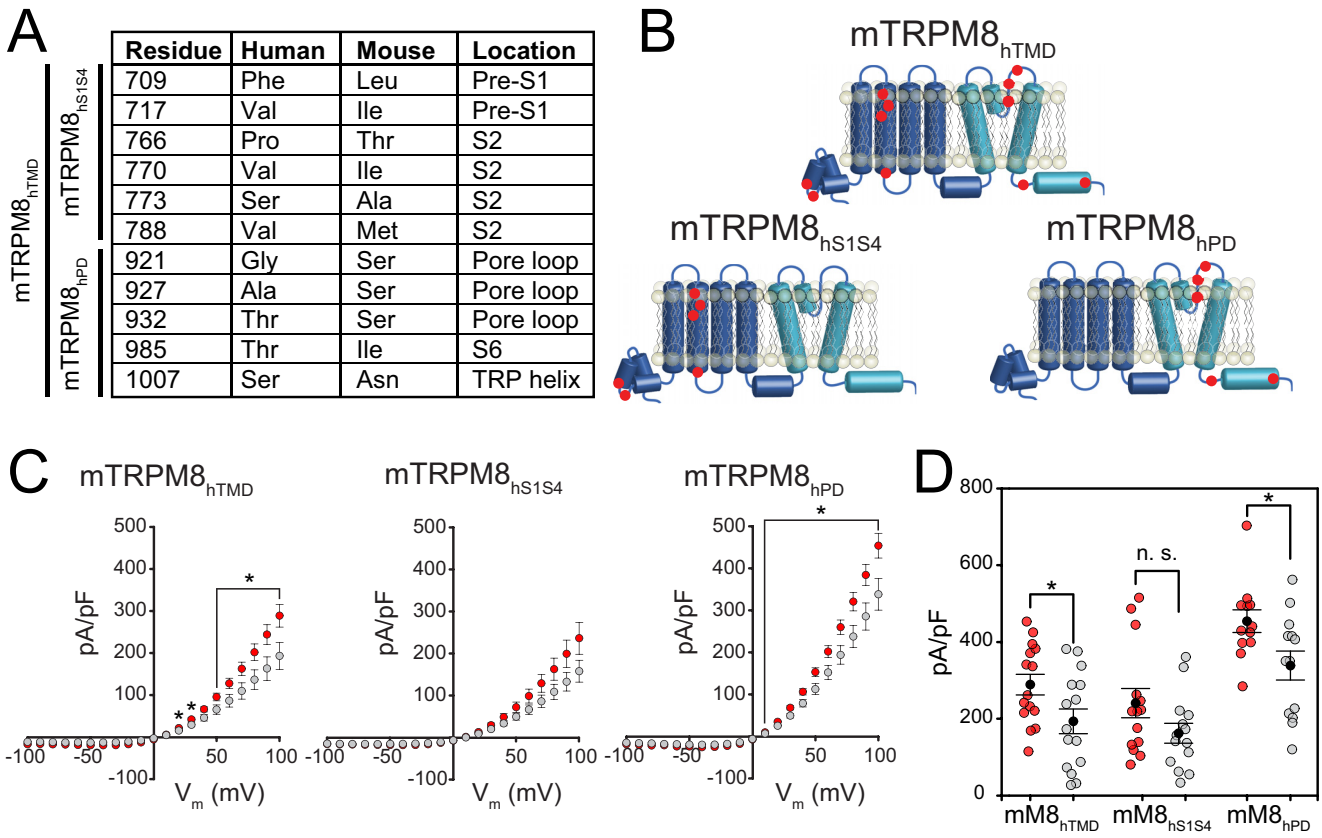

Figure 5. Mouse-human chimeric channels demonstrate functional determinants of TRPM8 modulation by PIRT. *A,* divergent residues in the transmembrane domains of human and mouse TRPM8. *B,* topology plots illustrating the locations of divergent residues in each chimeric construct. The full transmembrane domain has 11 mutations, the S1–S4 domain has six, and the pore domain has three. *C,* current-voltage plots showing attenuation of currents when chimeric channels are coexpressed with hPIRT. Measurements were made at ambient temperature (~23 °C) in the presence of 500 μM menthol ($mTRPM8_{hTMD}$, $n = 15$; $mTRPM8_{hTMD}$ + hPIRT, $n = 15$; $mTRPM8_{hS1S4}$, $n = 14$; $mTRPM8_{hS1S4}$ + hPIRT, $n = 14$; $mTRPM8_{hPD}$, $n = 12$; $mTRPM8_{hPD}$ + hPIRT, $n = 13$). *D,* jitter plot of steady-state current density from individual cells at +100 mV in the presence of 500 μM menthol. Human PIRT significantly attenuates the current response from $mTRPM8_{hTMD}$ and $mTRPM8_{hPD}$ chimeras. Average current from $mTRPM8_{hS1S4}$ channels is also lower but not to a significant degree. All *error bars* represent mean ± S.E. *Red circles* represent cells transfected with a *TRPM8* chimera and vector, *gray circles* represent cells transfected with a *TRPM8* chimera and human *PIRT*, and *black circles* represent average current density.

ond study by Gordon and co-workers (23) used a Förster resonance energy transfer (FRET) approach where fluorescent proteins were genetically fused to the termini of TRPV1 and PIRT and the fluorescent signal was measured in HEK-293 cells. No FRET signal was observed; nevertheless, the lack of FRET signal does not necessarily rule out an association between the proteins, as this negative result could potentially occur for a number of reasons, such as suboptimal structural arrangement of the fluorophores (23). The lack of FRET could arise because the fluorophore was fused to the C terminus of PIRT, which is implicated in TRP channel binding (14). Also, given the relatively small size of PIRT (~15 kDa) compared with the size of the YFP fluorophore (~26 kDa), it is possible that the C-terminal tag could sterically interfere with the TRPV1–PIRT interaction.

Our data indicate that the TRPM8 S1–S4 domain binds specifically with PIRT in a 1:1 binding stoichiometry. This association is demonstrated using two different methods that show a direct interaction between the two proteins. In functioning TRP channels, the S1–S4 domain is positioned at the periphery of the tetrameric channel with the conducting pore in the center. The molecular mechanism of TRP channel gating is currently under investigation; however, the gating mechanism of similarly structured voltage-gated potassium (K_V) channels is better established. It is known that the S4 helix within the voltage-sensing domain of K_V channels is responsible for opening the gate upon membrane depolarization (28). Thus from an evolutionary standpoint it is possible that the structurally homologous S1–S4 domain of TRP channels is involved in channel gating. Recent studies of TRPM8 and TRPV1 identify the respective S1–S4 domains as central to ligand binding and activation (29, 30). The 1:1 stoichiometry we observed suggests a possible mechanism of fine-tuning TRPM8 activity; each channel has four S1–S4 domains, so it may be possible that up to four PIRT proteins can interact with the channel (Fig. 6). Different levels of PIRT expression could result in varying degrees of attenuation for the human channel (or activation for the mouse channel), as has recently been shown with K_V channel-interacting proteins (31).

Mounting evidence points to the complex role of regulatory proteins in TRP channel function. Gkika *et al.* (22) recently reported a family of TRPM8-associated proteins found in prostate cells. These TRP channel-associated factors regulate TRPM8 trafficking to the plasma membrane as well as kinetic states at the single channel level (22). Weng *et al.* (32) reported that a protein known as Tmem100 enhances TRPA1 activity by

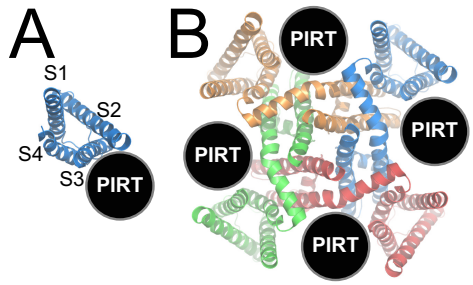

Figure 6. A model of PIRT–TRPM8 complex stoichiometry. *A,* based on NMR titration data, PIRT binds the TRPM8 S1–S4 domain with a 1:1 stoichiometry. *B,* functional channels are homotetramers, suggestive that up to four PIRT proteins can simultaneously bind TRPM8. Thus, the number of PIRT proteins bound is a possible mechanism of further fine-tuning the channel activity.

modulating the physical association of a TRPA1–TRPV1 complex, thus interfering with TRPV1-mediated inhibition of TRPA1. Interestingly, a Tmem100 mutant was found to have the inverse effect, inhibiting TRPA1 activity by enhancing the association between TRPA1 and TRPV1 (32). Based on this result, a synthetic peptide mimicking the Tmem100 mutant was designed and found to reduce pain behaviors induced by mustard oil, a TRPA1 agonist (32). Like PIRT, Tmem100 is a small two-span membrane protein and is evolutionarily related to PIRT with 27% sequence identity between the human paralogs. In addition to TRP channel function being modulated by proteins like TRP channel-associated factors and PIRTs, there is emerging evidence that PIRT is an endogenous regulator of P2X purinergic receptors (16, 33). As with TRP channels, P2X receptors are considered promising therapeutic targets and highlight the possibility of developing therapeutics based on targeting modulatory proteins such as PIRT.

In addition to TRP channels, many ion channels have been shown to be regulated by modulatory subunits. The voltage-sensitive channel KCNQ1 (K_V7.1) is regulated in diverse ways by KCNE subunits, which are single span integral membrane proteins (34). The five members of the KCNE family are known to modulate multiple different K_V channels, resulting in changes in properties including current density, pharmacology, and activation and inactivation kinetics (35). For example, KCNQ1 activation is dramatically slowed and current density increased when associated with KCNE1, whereas KCNE4 completely abolishes KCNQ1 currents (36, 37). This functional relationship is further complicated by the fact that KCNE1 and KCNE4 can also co-associate with KCNQ1 to form heteromultimeric complexes (38). Mutations in these subunits disrupt native currents and are associated with inherited cardiac arrhythmias including long QT syndrome, underscoring the physiological importance of ion channel modulation (39). Another example is the β-subunits of BK channels (34). In cochlear hair cells, differential expression of β1 and β4 subunits is a mechanism of tuning BK channels to facilitate appropriate electrical oscillation frequency (40, 41), whereas the β2 subunit is responsible for inactivating BK channels in adrenal chromaffin cells (42). Regulation by modulatory proteins is a well-established mechanism of enhanced functional diversity of ion channels; a single type of channel can be adapted for different roles in different tissue or cell types. TRP channels are likewise widely expressed and have diverse physiological roles; modulatory proteins like PIRT and Tmem100 (PIRT2) appear to be an additional mechanism that enhances functional diversity.

Previous studies have shown that the C terminus of PIRT binds to both TRPV1 and TRPM8, and the PIRT C terminus also binds to PIP_2, a known regulator of TRP channel function (4, 14, 23). In particular, the proximal C terminus of TRPV1 has been implicated in regulation by PIP_2 (23). A FRET-based assay using the proximal C-terminal region fused to a cyan fluorescent protein showed a FRET signal when mixed with fluorescently labeled PIP_2, indicating that this region binds PIP_2. Deletion or neutralization of basic residues in this region eliminated TRPV1 capsaicin-activated currents; however, it was unclear whether this was due to disruption of PIP_2 binding or unrelated changes in channel trafficking or function. Cryo-EM structures of TRPV1 provide additional insight; the PIP_2-binding region identified by Gordon and co-workers (23) is found at the end of a juxtamembrane helix following the S6 helix, near a region that is conserved in TRP channels called the TRP box, which protrudes beneath the S1–S4 domain (43). This supports the notion that the S1–S4 domain might be involved in channel regulation by PIP_2. The proximal C-terminal region of TRPV1 has also been shown to bind to PIP_2; this region is conserved across TRPV and TRPM channel families, and so the mechanism of PIP_2 regulation may also be conserved (4, 23).

Our data show that PIRT binds specifically to the TRPM8 S1–S4 domain. Recently, cryo-EM structures of TRP channels from all subfamilies have become available. A general feature of these structures is that the aforementioned proximal C-terminal putative PIP_2-binding site extends beneath the S1–S4 domain, placing them in close proximity. Also, TRPV family studies recently identified a potentially distinct phosphoinositide-binding site where PIP_2 binds residues in the S4 helix and S4–S5 linker of PIP_2-sensitive TRPV family channels (44, 45). Taken together, these results suggest a possible regulatory mechanism in which PIRT and PIP_2 interact and exert their modulatory effects near the S1–S4 domain. Our data also suggest possible differences in channel activation mechanisms between cold, menthol, and voltage stimulation. Under cold stimulation, hPIRT expression resulted in attenuated current response even at physiological negative voltages (Fig. 1*C*), whereas menthol and room temperature currents were only affected at positive voltages (Fig. 1, *A* and *B*).

The transmembrane domain of TRP channels is an important functional nexus. For example, recent studies have elucidated that TRPM8-mediated thermosensitivity species differences in hibernating rodents can be recapitulated by swapping only six residues within the TRPM8–TMD, similar to the number of divergent residues between mouse and human TRPM8 in our experiments (24). Previous studies have shown that species differences between a small number of residues in the transmembrane core give rise to capsaicin sensitivity in TRPV1 and icilin sensitivity in TRPM8 (19, 25). Additionally, the transmembrane domain of TRPA1 is sufficient to recapitulate temperature and agonist response of this channel (46, 47). Given the importance of the transmembrane core in TRP channel function, we focused our search on this region. Human and mouse TRPM8 have few sequence differences, but electrophys-

iology measurements from chimeric channels demonstrate that these few differences have significant functional consequences. Swapping the 11 human mutations in the transmembrane core produced a channel that recapitulated the human phenotype of TRPM8 attenuation by hPIRT, indicating key functional determinants are found in these residues. Narrowing the chimeric region to the S1–S4 domain resulted in somewhat attenuated currents, whereas the pore domain chimera had significantly attenuated currents. Considering these results together with our data showing that PIRT binds the TRPM8 S1–S4 domain, it is possible that this domain is important for binding, whereas most of the functional effect is produced in the pore domain.

Besides interactions with hPIRT, swapping the three disparate residues found in the pore loop and TRP helix of hTRPM8 into mTRPM8 produced a channel that exhibited significantly increased overall current magnitudes compared with the TMD and S1–S4 domain chimeras. The region these residues are found is unresolved in the *F. albicollis* TRPM8 cryo-EM structure, but it is clear they are in the pore loop following the pore helix (27). In structures of TRPM4, where equivalent post pore helix residues are resolved, these residues are outside of the selectivity filter, so they likely do not directly determine channel conductance (48–50). It is noteworthy that this increase in conductance is not seen in the $mTRPM8_{hTMD}$ chimera, which also includes the pore loop and TRP helix changes. This is possibly a consequence of the spatial arrangement of these residues, as the TRP helix extends beneath the S1–S4 domain and plays a key role in channel gating regulation (27).

Species divergence has been well-documented in other TRP channels (18–20, 51, 52). In particular, TRPM8 orthologs have significant differences in temperature sensitivity as a result of species-specific evolutionary pressure from environmental factors and thermoregulation (20, 24, 53). Given this speciation it seems likely that a modulatory protein like PIRT would also be under evolutionary pressure to fine-tune a given TRP channel for a particular environmental niche. As PIRT is expressed exclusively in the peripheral nervous system (14), its physiological interaction with TRPM8 may be limited to modulating thermosensation, and the differences between modulation of human and mouse TRPM8 by PIRT could reflect the different thermosensation requirements of the two species.

TRP channels, including TPRM8 are functionally diverse both within an organism and across species. Small modulatory proteins such as PIRT may provide a partial explanation for how a single TRP channel is physiologically repurposed for a variety of cellular needs.

Experimental procedures

Cell culture

HEK-293 cells (ATCC CRL-1573) were authenticated by polymorphic genetic marker testing (DNA Diagnostics Center Medical). Cells were cultured in growth medium consisting of 90% Dulbecco's modified Eagle's medium, 10% fetal bovine serum, 100 units ml^{-1} of penicillin-streptomycin, and 2 mM L-glutamine (Gibco). Cells were cultured in 35-mm polystyrene dishes (Falcon) and experiments were conducted at 37 °C in the presence of 5% CO_2. Cells were transiently co-transfected with human or mouse gene orthologs of pIRES2–TRPM8–EGFP and either ortholog of pIRES2–PIRT–DsRed or, as a negative control, the empty pIRES2–DsRed plasmid. These constructs express bicistronic mRNA with an internal ribosome entry site (IRES) positioned between the gene of interest (*TRPM8* or *PIRT*) and the fluorescent protein reporter gene (*EGFP* or *DsRed*) such that the reporter is not covalently fused to the protein of interest. Transient transfection was achieved using FuGENE 6 transfection reagent (Promega) and 0.5 μg of each plasmid in a 35-mm dish (Falcon) at a ratio of 3 μl of transfection reagent per μg of plasmid.

Electrophysiology measurements

Forty-eight hours after transfection, cells were released from culture dishes by brief exposure to 0.25% trypsin/EDTA and resuspended in supplemented DMEM; cells were then plated on glass coverslips and allowed to recover for 1–2 h at 37 °C in 5% CO_2. Cells that exhibited yellow (green and red markers) fluorescence, indicating successful co-transfection of both plasmids, were selected for electrophysiology measurements. Whole-cell voltage-clamp current measurements were performed using an Axopatch 200B amplifier (Axon Instruments) and pClamp 10.3 software (Axon Instruments). Data were acquired at 2 kHz and filtered at 1 kHz. Patch pipettes were pulled using a P-2000 laser puller (Sutter Instruments) from borosilicate glass capillaries (World Precision Instruments) and heat-polished using a MF-830 microforge (Narishige). Pipettes had resistances of 2–5 megohms in the extracellular solution. A reference electrode was placed in a 2% agar bridge made with a composition similar to the extracellular solution. Experiments were performed at 23 ± 1 °C unless otherwise noted. Cells were placed in a chamber with extracellular solution containing (in mM) NaCl 132, KCl 4.8, $MgCl_2$ 1.2, $CaCl_2$ 2, HEPES 10, and glucose 5, with the pH adjusted to 7.4 using NaOH and the osmolality adjusted to 310 mosmol using sucrose. Pipettes were filled with a solution containing (in mM) K^+ gluconate 135, KCl 5, $MgCl_2$ 1, EGTA 5, and HEPES 10; pH was adjusted to 7.2 with KOH, and osmolality was adjusted to 300 mosmol using sucrose. Chemicals were obtained from Sigma. Osmolality was measured using a Vapro 5600 vapor pressure osmometer (Wescor). At least 15 cells were recorded for each condition. Unpaired two-tailed Student's *t* tests were performed to determine statistical significance, and differences were considered significant at $p < 0.05$ as indicated by a single asterisk (*). A double or triple asterisk indicates $p < 0.01$ or $p < 0.001$, respectively.

For temperature-controlled experiments, extracellular solution was cooled using a Peltier-based perfusion system (ALA Scientific). For menthol perfusion experiments, a menthol stock solution was prepared by dissolving menthol in DMSO at a concentration of 100 mg ml^{-1}. This stock was then diluted with extracellular solution to 500 μM menthol.

Cell-surface expression

A C-terminal human influenza hemagglutinin (HA) epitope-tagged construct of hTRPM8 was generated. The tag sequence was as follows: YPYDVPDYA. An additional glycine residue

was added before the tag sequence to promote structural flexibility. Functionality of the construct was verified by cold and menthol sensitivity in whole-cell patch clamp experiments where it behaved like WT TRPM8 (data not shown). HEK-293 cells were cultured in 100-mm dishes as described above. Three sets of five dishes were transfected with pIRES2–hTRPM8–HA–EGFP/pIRES2–hPIRT–DsRed, pIRES2–hTRPM8–HA–EGFP/pIRES2–DsRed (a positive control), or empty vectors (pIRES2–EGFP/pIRES2–DsRed, a negative control). After ~42 h, cells were washed twice with cold PBS (pH 7.4) and incubated with agitation in 0.5 mg ml^{-1} sulfo-NHS-SS-biotin (Thermo Scientific) in PBS for 30 min at 4 °C. Cells were further washed three times in cold PBS, incubated with quenching solution (100 mM glycine in PBS) for 5 min, and then washed two additional times with cold PBS. Cells were lysed in 600 μl of RIPA buffer (150 mM NaCl, 5 mM EDTA, 50 mM Tris, 1% Nonidet P-40 substitute (4-nonylphenyl-PEG), 0.5% sodium deoxycholate, 0.1% SDS, pH 7.4) and incubated with tumbling at 4 °C for 15 min. Lysate was centrifuged for 10 min at 14,000 × *g* at 4 °C. Protein concentration of the lysate was measured by BCA assay (Thermo Fisher), and a normalized volume of lysate was added to 150 μl (75 μl bed volume) of NeutrAvidin UltraLink resin (Thermo Scientific). Lysate was tumbled overnight at 4 °C. Supernatant was collected, and resin was washed with RIPA buffer. Surface-expressed biotinylated protein was eluted in 2× SDS-PAGE loading dye and analyzed by SDS-PAGE and Western blotting.

For hTRPM8 detection, the membrane was probed with a mouse monoclonal anti-HA primary antibody (Thermo catalogue number 26183, lots QK218547 and SA244939) diluted to 1:1000. For loading control, mouse anti-β-actin primary antibody (Thermo catalogue number MA5–15739, lots QH220961 and SF253548) was diluted to 1:2000. In both cases, horse anti-mouse IgG secondary antibody (Cell Signaling Technology catalogue numbers 7076, lot 32) was diluted to 1:1500. Blots were developed with Clarity ECL blotting substrate (Bio-Rad) according to the manufacturer's protocol. Blots were imaged using a Nikon D610 DSLR camera and Nikkor 50-mm f/1.4G lens and processed using Photoshop (54). In an effort to minimize experimental bias, the trafficking studies are from three independent sets of experiments that were carried out on independently transfected dishes of cells on different days.

Chimera generation

Human and mouse TRPM8 sequences were aligned using Clustal Omega. Chimeric regions were swapped with the pIRES2 vector using MEGAWHOP PCR (55). The initial primer sequences for generating megaprimers are as follows: $mTRPM8_{hTMD}$: forward, GTCTATTCATTATCCCCTTAGTGGGCTGTGGCTTTGTATCATTTAG; reverse, GACAACGAAGGGGAAGGGGATGTTTAGGCGGCTGCAGTACTCCTGCAC; $mTRPM8_{hS1S4}$: forward, GTCTATTCATTATCCCCTTAGTGGGCTGTGGCTTTGTATCATTTAG; reverse, AACGTTCCATAGGTCGGTGAAATAATTCACTCCGTTTACGTACCACTGTCTCACTTC; $mTRPM8_{hPD}$: forward, GGAGATGGATCTTCCGCTCTGTCATCTATGAGCCCTACCTGGCCATGTTC; reverse, GACAACGAAGGGGAAGGGGATGTTTAGGCGGCTGCAGTACTCCTGCAC. Megaprimers were generated using PCR and purified using an agarose gel purification kit (Qiagen). Purified chimera plasmid DNA were verified by Sanger sequencing and transfected into HEK-293 cells for electrophysiology experiments as described above.

Expression and purification of hTRPM8 S1–S4 domain and hKCNQ1–VSD

Overexpression of the hTRPM8 S1–S4 domain was carried out as previously described and used in PIRT binding studies (29). Briefly, N-terminal His_{10}-tagged hTRPM8 S1–S4 domain was expressed and purified using a Ni^{2+}-NTA column. The His_{10} tag was removed by cleaving with restriction grade thrombin (Novagen). Following thrombin cleavage, the hTRPM8 S1–S4 domain was again flowed over a Ni^{2+}-NTA column to eliminate the uncleaved His_{10}–hTRPM8 S1–S4 domain. The voltage-sensing domain of the human KCNQ1 potassium channel (hKCNQ1–VSD) was expressed and purified according to a previously published protocol and used as a negative control in PIRT NMR binding studies (56).

Expression and purification of hPIRT

Recombinant hPIRT was expressed with a His_6 tag on the N terminus in a pET16b vector and grown in BL21 Star (DE3) *Escherichia coli* at 25 °C in M9 minimal media with 100 μg/ml of ampicillin and enriched with 1 g/liter of (^{15}N) ammonium chloride. 0.5 mM Isopropyl 1-thio-β-D-galactopyranoside was used to induce expression of hPIRT at $OD_{600\ nm}$ of 0.6, and cells were allowed to express for 20 h.

Cells were harvested by 6,000 × *g* centrifugation at 4 °C. The resulting cell pellets were resuspended in a lysis buffer (75 mM Tris-HCl, 300 mM NaCl, 0.2 mM EDTA, pH 7.7) with 20 ml/g of cell pellet. Lysozyme (0.2 mg/ml), RNase (0.02 mg/ml), DNase (0.02 mg/ml), 1 mM phenylmethanesulfonyl fluoride (Sigma), and 5 mM magnesium acetate were added and the solution was tumbled for 30 min at room temperature. Cells were then lysed by sonication using a Misonix Ultrasonic Liquid Processor at 4 °C with a 50% duty cycle (5 s on, 5 s delay). Empigen (Sigma) was then added to 3.5% (v/v) and the lysate was allowed to rotate at 4 °C for 30 min. The cellular lysate was then centrifuged for 20 min at 20,000 × *g*; the pellet was then discarded and the supernatant was used for PIRT purification. Ni-NTA Superflow resin (Qiagen; 2 ml of resin/g of cell pellet) was added to the supernatant and allowed to rotate at 4 °C for 30 min. The resin and supernatant mixture were then packed into a chromatography column and washed with 10 column volumes of primary buffer (40 mM HEPES, 300 mM NaCl, 3% (v/v) Empigen, pH 7.5). Ten column volumes of secondary buffer (1.5% Empigen, 30 mM imidazole, 40 mM HEPES, 300 mM NaCl, pH 7.5) was then used to wash nonspecific binding proteins from the resin. This was followed by 5 column volumes of tertiary buffer (0.2% DPC, 25 mM sodium phosphate, pH 7.2) used to exchange detergents from Empigen to dodecylphosphocholine (DPC, Avanti Polar Lipids). Last, the protein was eluted from the resin with an elution buffer (0.5% DPC, 300 mM imidazole, 25 mM sodium phosphate, pH 7.8). All of the buffers used for chromatography contained 2.2 mM β-mercaptoethanol (Sigma) that was added immediately prior to purification.

Following nickel affinity chromatography, hPIRT was subjected to ion exchange chromatography. The high concentration of imidazole, 300 mM, was decreased to <1 mM by ultrafiltration, using an Amicon Ultra-15 centrifugal filter unit with 10-kDa cutoff. The protein solution was then bound to a 1-ml cation exchange column (GE Healthcare, HiTrap SP FF) using an AKTA Pure FPLC with low salt buffer (0.2% DPC, 50 mM HEPES, 50 mM NaCl, pH 7.5) and eluted with high salt buffer (0.5% DPC, 50 mM HEPES, 1 M NaCl, pH 7.5). After purification steps, total yield of hPIRT was ~2 mg/liter of minimal media. For NMR experiments, the resulting eluent was then buffer exchanged to phosphate buffer (20 mM sodium phosphate, 0.5 mM EDTA, and pH 6.5) using an Amicon Ultra-4 centrifugal filter unit with 10-kDa cutoff to a final volume of 180 μl with a resulting concentration of 0.5 mM protein. The sample plus 4 μl (2% v/v) of D_2O were loaded into a 3-mm NMR tube (Bruker).

hTRPM8 S1–S4 domain and hPIRT pulldown experiment

To test whether the hTRPM8 S1–S4 domain and hPIRT directly interact *in vitro*, the hTRPM8 S1–S4 domain and His_6–hPIRT were expressed in *E. coli* and purified in 25 mM Na_2HPO_4 (pH 7.3) containing ~1% DPC (about 28 mM which is about 19 times the critical micelle concentration). 50 μg each of hTRPM8 S1–S4 domain (after thrombin cleavage and removal of the ×10 His tag) and His_6–hPIRT were mixed with continuous tumbling for 12 h at room temperature. This was followed by incubation with 100 μl of Ni-NTA resin for 2 h at room temperature. After Ni-NTA interaction, unbound protein in the supernatant was separated by centrifugation at 3000 × *g* for 2 min using a benchtop centrifuge (Thermo Scientific). Protein-bound Ni-NTA resin was washed with 6 ml (60 column volumes) of 25 mM Na_2HPO_4 (pH 7.3) buffer containing 0.25% DPC (w/v, ~7 mM) followed by elution of the bound protein using the same buffer containing 500 mM imidazole. The eluted protein fractions were analyzed on 16% Tris glycine SDS-PAGE.

hPIRT– hTRPM8 S1–S4 domain and KCNQ1–VSD NMR titration

For ^{15}N-labeled hPIRT, ^{1}H,^{15}N-TROSY-HSQC experiments were acquired at 40 °C on a Bruker 850 MHz (^{1}H) spectrometer with a helium cooled 5-mm TCI cryoprobe and Avance III HD console. 128 transients, with 2048 points in the direct and 128 points in the indirect dimension, of hPIRT without the hTRPM8 S1–S4 domain were recorded and analyzed as the initial titration point. After the initial titration point was recorded, the sample was removed and the TRPM8 S1–S4 domain added to the desired mole ratio and concentrated to 180 μl; iterations of this were done to produce several titration points at mole ratios ranging from 0:1 to 2:1 hTRPM8 S1–S4 domain:hPIRT. As a negative control, the same protocol was performed with the KCNQ1–VSD.

NMR data were processed in NMRPipe and analyzed with CcpNmr analysis (57, 58). The change in chemical shifts ($\Delta\delta$) were plotted and compared with reference resonances, where $\Delta\delta = [((\Delta\delta_H)^2 + [0.2((\Delta\delta_N)]^2]^{1/2}$. Dissociation constants were extracted using the *nlinfit* function in *Matlab R2013a* and a single binding site model with the equation: $f(x) = (x)(B_{max})/(K_d + x)$, where B_{max} is the maximal change in chemical shift observed for a given resonance upon saturation with ligand (hTRPM8 S1–S4 domain), K_d is the dissociation constant, x is the hTRPM8 S1–S4 domain:hPIRT ratio, and $f(x)$ is correlated to the absolute value of the change in chemical shift ($\Delta\delta$).

Author contributions—J. K. H., T. S., N. J. S., P. R., and W. D. V. H. data curation; J. K. H. and W. D. V. H. formal analysis; J. K. H. and W. D. V. H. investigation; J. K. H. and W. D. V. H. methodology; J. K. H. and W. D. V. H. writing-original draft; J. K. H., N. J. S., P. R., and W. D. V. H. writing-review and editing; W. D. V. H. conceptualization; W. D. V. H. funding acquisition; W. D. V. H. validation.

Acknowledgment—We thank Prof. Charles Sanders (Vanderbilt University) for providing the KCNQ1 voltage-sensing domain plasmid.

References

1. McKemy, D. D., Neuhausser, W. M., and Julius, D. (2002) Identification of a cold receptor reveals a general role for TRP channels in thermosensation. *Nature* **416,** 52–58 CrossRef Medline
2. Peier, A. M., Moqrich, A., Hergarden, A. C., Reeve, A. J., Andersson, D. A., Story, G. M., Earley, T. J., Dragoni, I., McIntyre, P., Bevan, S., and Patapoutian, A. (2002) A TRP channel that senses cold stimuli and menthol. *Cell* **108,** 705–715 CrossRef Medline
3. Andersson, D. A., Chase, H. W., and Bevan, S. (2004) TRPM8 activation by menthol, icilin, and cold is differentially modulated by intracellular pH. *J. Neurosci.* **24,** 5364–5369 CrossRef Medline
4. Rohacs, T. (2014) Phosphoinositide regulation of TRP channels. *Handb. Exp. Pharmacol.* **223,** 1143–1176 CrossRef Medline
5. Knowlton, W. M., Daniels, R. L., Palkar, R., McCoy, D. D., and McKemy, D. D. (2011) Pharmacological blockade of TRPM8 ion channels alters cold and cold pain responses in mice. *PloS One* **6,** e25894 CrossRef Medline
6. Almeida, M. C., Hew-Butler, T., Soriano, R. N., Rao, S., Wang, W., Wang, J., Tamayo, N., Oliveira, D. L., Nucci, T. B., Aryal, P., Garami, A., Bautista, D., Gavva, N. R., and Romanovsky, A. A. (2012) Pharmacological blockade of the cold receptor TRPM8 attenuates autonomic and behavioral cold defenses and decreases deep body temperature. *J. Neurosci.* **32,** 2086–2099 CrossRef Medline
7. Ding, Z., Gomez, T., Werkheiser, J. L., Cowan, A., and Rawls, S. M. (2008) Icilin induces a hyperthermia in rats that is dependent on nitric oxide production and NMDA receptor activation. *Eur. J. Pharmacol.* **578,** 201–208 CrossRef Medline
8. Gavva, N. R., Davis, C., Lehto, S. G., Rao, S., Wang, W., and Zhu, D. X. (2012) Transient receptor potential melastatin 8 (TRPM8) channels are involved in body temperature regulation. *Mol. Pain* **8,** 36 Medline
9. Ma, S., Yu, H., Zhao, Z., Luo, Z., Chen, J., Ni, Y., Jin, R., Ma, L., Wang, P., Zhu, Z., Li, L., Zhong, J., Liu, D., Nilius, B., and Zhu, Z. (2012) Activation of the cold-sensing TRPM8 channel triggers UCP1-dependent thermogenesis and prevents obesity. *J. Mol. Cell. Biol.* **4,** 88–96 CrossRef Medline
10. Sun, J., Yang, T., Wang, P., Ma, S., Zhu, Z., Pu, Y., Li, L., Zhao, Y., Xiong, S., Liu, D., and Zhu, Z. (2014) Activation of cold-sensing transient receptor potential melastatin subtype 8 antagonizes vasoconstriction and hypertension through attenuating RhoA/Rho kinase pathway. *Hypertension* **63,** 1354–1363 CrossRef Medline
11. Quallo, T., Vastani, N., Horridge, E., Gentry, C., Parra, A., Moss, S., Viana, F., Belmonte, C., Andersson, D. A., and Bevan, S. (2015) TRPM8 is a neuronal osmosensor that regulates eye blinking in mice. *Nat. Commun.* **6,** 7150 CrossRef Medline
12. Tang, Z., Kim, A., Masuch, T., Park, K., Weng, H., Wetzel, C., and Dong, X. (2013) Pirt functions as an endogenous regulator of TRPM8. *Nat. Commun.* **4,** 2179 Medline
13. Tang, M., Wu, G. Y., Dong, X. Z., and Tang, Z. X. (2016) Phosphoinositide interacting regulator of TRP (Pirt) enhances TRPM8 channel activity *in vitro* via increasing channel conductance. *Acta Pharmacol. Sin.* **37,** 98–104 CrossRef Medline

14. Kim, A. Y., Tang, Z., Liu, Q., Patel, K. N., Maag, D., Geng, Y., and Dong, X. (2008) Pirt, a phosphoinositide-binding protein, functions as a regulatory subunit of TRPV1. *Cell* **133,** 475–485 CrossRef Medline
15. Wang, C., Wang, Z., Yang, Y., Zhu, C., Wu, G., Yu, G., Jian, T., Yang, N., Shi, H., Tang, M., He, Q., Lan, L., Liu, Q., Guan, Y., Dong, X., Duan, J., and Tang, Z. (2015) Pirt contributes to uterine contraction-induced pain in mice. *Mol. Pain* **11,** 57 Medline
16. Gao, X. F., Feng, J. F., Wang, W., Xiang, Z. H., Liu, X. J., Zhu, C., Tang, Z. X., Dong, X. Z., and He, C. (2015) Pirt reduces bladder overactivity by inhibiting purinergic receptor P2X3. *Nat. Commun.* **6,** 7650 CrossRef Medline
17. Patel, K. N., Liu, Q., Meeker, S., Undem, B. J., and Dong, X. (2011) Pirt, a TRPV1 modulator, is required for histamine-dependent and -independent itch. *PLoS ONE* **6,** e20559 CrossRef Medline
18. Hilton, J. K., Rath, P., Helsell, C. V., Beckstein, O., and Van Horn, W. D. (2015) Understanding thermosensitive transient receptor potential channels as versatile polymodal cellular sensors. *Biochemistry* **54,** 2401–2413 CrossRef Medline
19. Jordt, S.-E., and Julius, D. (2002) Molecular basis for species-specific sensitivity to "hot" chili peppers. *Cell* **108,** 421–430 CrossRef Medline
20. Myers, B. R., Sigal, Y. M., and Julius, D. (2009) Evolution of thermal response properties in a cold-activated TRP channel. *PLoS ONE* **4,** e5741 CrossRef Medline
21. Janssens, A., and Voets, T. (2011) Ligand stoichiometry of the cold- and menthol-activated channel TRPM8. *J. Physiol.* **589,** 4827–4835 CrossRef Medline
22. Gkika, D., Lemonnier, L., Shapovalov, G., Gordienko, D., Poux, C., Bernardini, M., Bokhobza, A., Bidaux, G., Degerny, C., Verreman, K., Guarmit, B., Benahmed, M., de Launoit, Y., Bindels, R. J., Fiorio Pla, A., and Prevarskaya, N. (2015) TRP channel-associated factors are a novel protein family that regulates TRPM8 trafficking and activity. *J. Cell Biol.* **208,** 89–107 CrossRef Medline
23. Ufret-Vincenty, C. A., Klein, R. M., Hua, L., Angueyra, J., and Gordon, S. E. (2011) Localization of the PIP2 sensor of TRPV1 ion channels. *J. Biol. Chem.* **286,** 9688–9698 CrossRef Medline
24. Matos-Cruz, V., Schneider, E. R., Mastrotto, M., Merriman, D. K., Bagriantsev, S. N., and Gracheva, E. O. (2017) Molecular prerequisites for diminished cold sensitivity in ground squirrels and hamsters. *Cell Rep.* **21,** 3329–3337 CrossRef Medline
25. Chuang, H. H., Neuhausser, W. M., and Julius, D. (2004) The super-cooling agent icilin reveals a mechanism of coincidence detection by a temperature-sensitive TRP channel. *Neuron* **43,** 859–869 CrossRef Medline
26. Kroncke, B. M., Van Horn, W. D., Smith, J., Kang, C., Welch, R. C., Song, Y., Nannemann, D. P., Taylor, K. C., Sisco, N. J., George, A. L., Jr., Meiler, J., Vanoye, C. G., and Sanders, C. R. (2016) Structural basis for KCNE3 modulation of potassium recycling in epithelia. *Sci. Adv.* **2,** e1501228 CrossRef Medline
27. Yin, Y., Wu, M., Zubcevic, L., Borschel, W. F., Lander, G. C., and Lee, S. Y. (2018) Structure of the cold- and menthol-sensing ion channel TRPM8. *Science* **359,** 237–241 CrossRef Medline
28. Jensen MØ., Jogini, V., Borhani, D. W., Leffler, A. E., Dror, R. O., and Shaw, D. E. (2012) Mechanism of voltage gating in potassium channels. *Science* **336,** 229–233 CrossRef Medline
29. Rath, P., Hilton, J. K., Sisco, N. J., and Van Horn, W. D. (2016) Implications of human transient receptor potential melastatin 8 (TRPM8) channel gating from menthol binding studies of the sensing domain. *Biochemistry* **55,** 114–124 CrossRef Medline
30. Yang, F., Xiao, X., Cheng, W., Yang, W., Yu, P., Song, Z., Yarov-Yarovoy, V., and Zheng, J. (2015) Structural mechanism underlying capsaicin binding and activation of the TRPV1 ion channel. *Nat. Chem. Biol.* **11,** 518–524 CrossRef Medline
31. Zhou, J., Tang, Y., Zheng, Q., Li, M., Yuan, T., Chen, L., Huang, Z., and Wang, K. (2015) Different KChIPs compete for heteromultimeric assembly with pore-forming Kv4 subunits. *Biophys. J.* **108,** 2658–2669 CrossRef Medline
32. Weng, H. J., Patel, K. N., Jeske, N. A., Bierbower, S. M., Zou, W., Tiwari, V., Zheng, Q., Tang, Z., Mo, G. C., Wang, Y., Geng, Y., Zhang, J., Guan, Y., Akopian, A. N., and Dong, X. (2015) Tmem100 is a regulator of TRPA1-TRPV1 complex and contributes to persistent pain. *Neuron* **85,** 833–846 CrossRef Medline
33. Guo, W., Sui, Q. Q., Gao, X. F., Feng, J. F., Zhu, J., He, C., Knight, G. E., Burnstock, G., and Xiang, Z. (2016) Co-localization of Pirt protein and P2X2 receptors in the mouse enteric nervous system. *Purinergic Signal.* **12,** 489–496 CrossRef Medline
34. Sun, X., Zaydman, M. A., and Cui, J. (2012) Regulation of voltage-activated K^+ channel gating by transmembrane β subunits. *Front. Pharmacol.* **3,** 63 Medline
35. McCrossan, Z. A., and Abbott, G. W. (2004) The MinK-related peptides. *Neuropharmacology* **47,** 787–821 CrossRef Medline
36. Barhanin, J., Lesage, F., Guillemare, E., Fink, M., Lazdunski, M., and Romey, G. (1996) K_VLQT1 and IsK (minK) proteins associate to form the I_{Ks} cardiac potassium current. *Nature* **384,** 78–80 CrossRef Medline
37. Grunnet, M., Jespersen, T., Rasmussen, H. B., Ljungstrøm, T., Jorgensen, N. K., Olesen, S.-P., and Klaerke, D. A. (2002) KCNE4 is an inhibitory subunit to the KCNQ1 channel. *J. Physiol.* **542,** 119–130 CrossRef Medline
38. Manderfield, L. J., and George, A. L., Jr. (2008) KCNE4 can co-associate with the I_{Ks} (KCNQ1-KCNE1) channel complex. *FEBS J.* **275,** 1336–1349 CrossRef Medline
39. Abbott, G. W., and Goldstein, S. A. (2002) Disease-associated mutations in KCNE potassium channel subunits (MiRPs) reveal promiscuous disruption of multiple currents and conservation of mechanism. *FASEB J.* **16,** 390–400 CrossRef Medline
40. Ramanathan, K., Michael, T. H., Jiang, G.-J., Hiel, H., and Fuchs, P. A. (1999) A molecular mechanism for electrical tuning of cochlear hair cells. *Science* **283,** 215–217 CrossRef Medline
41. Bai, J. P., Surguchev, A., and Navaratnam, D. (2011) β4-Subunit increases Slo responsiveness to physiological Ca^{2+} concentrations and together with β1 reduces surface expression of Slo in hair cells. *Am. J. Physiol. Cell Physiol.* **300,** C435–446 CrossRef Medline
42. Martinez-Espinosa, P. L., Yang, C., Gonzalez-Perez, V., Xia, X. M., and Lingle, C. J. (2014) Knockout of the BK β2 subunit abolishes inactivation of BK currents in mouse adrenal chromaffin cells and results in slow-wave burst activity. *J. Gen. Physiol.* **144,** 275–295 CrossRef Medline
43. Liao, M., Cao, E., Julius, D., and Cheng, Y. (2013) Structure of the TRPV1 ion channel determined by electron cryo-microscopy. *Nature* **504,** 107–112 CrossRef Medline
44. Gao, Y., Cao, E., Julius, D., and Cheng, Y. (2016) TRPV1 structures in nanodiscs reveal mechanisms of ligand and lipid action. *Nature* **534,** 347–351 CrossRef Medline
45. Velisetty, P., Borbiro, I., Kasimova, M. A., Liu, L., Badheka, D., Carnevale, V., and Rohacs, T. (2016) A molecular determinant of phosphoinositide affinity in mammalian TRPV channels. *Sci. Rep.* **6,** 27652 CrossRef Medline
46. Survery, S., Moparthi, L., Kjellbom, P., Högestatt, E. D., Zygmunt, P. M., and Johanson, U. (2016) The N-terminal ankyrin repeat domain is not required for electrophile and heat activation of the purified mosquito TRPA1 receptor. *J. Biol. Chem.* **291,** 26899–26912 CrossRef Medline
47. Moparthi, L., Survery, S., Kreir, M., Simonsen, C., Kjellbom, P., Högestatt, E. D., Johanson, U., and Zygmunt, P. M. (2014) Human TRPA1 is intrinsically cold- and chemosensitive with and without its N-terminal ankyrin repeat domain. *Proc. Natl. Acad. Sci. U.S.A.* **111,** 16901–16906 CrossRef Medline
48. Winkler, P. A., Huang, Y., Sun, W., Du, J., and Lü, W. (2017) Electron cryo-microscopy structure of a human TRPM4 channel. *Nature* **552,** 200–204 Medline
49. Duan, J., Li, Z., Li, J., Santa-Cruz, A., Sanchez-Martinez, S., Zhang, J., and Clapham, D. E. (2018) Structure of full-length human TRPM4. *Proc. Natl. Acad. Sci. U.S.A.* **115,** 2377–2382 CrossRef Medline
50. Autzen, H. E., Myasnikov, A. G., Campbell, M. G., Asarnow, D., Julius, D., and Cheng, Y. (2018) Structure of the human TRPM4 ion channel in a lipid nanodisc. *Science* **359,** 228–232 CrossRef Medline
51. Saito, S., Fukuta, N., Shingai, R., and Tominaga, M. (2011) Evolution of vertebrate transient receptor potential vanilloid 3 channels: opposite temperature sensitivity between mammals and Western clawed frogs. *PLoS Genet.* **7,** e1002041 CrossRef Medline

52. Chen, J., Kang, D., Xu, J., Lake, M., Hogan, J. O., Sun, C., Walter, K., Yao, B., and Kim, D. (2013) Species differences and molecular determinant of TRPA1 cold sensitivity. *Nat. Commun.* **4,** 2501 Medline
53. Gracheva, E. O., and Bagriantsev, S. N. (2015) Evolutionary adaptation to thermosensation. *Curr. Opin. Neurobiol.* **34,** 67–73 CrossRef Medline
54. Khoury, M. K., Parker, I., and Aswad, D. W. (2010) Acquisition of chemiluminescent signals from immunoblots with a digital single-lens reflex camera. *Anal. Biochem.* **397,** 129–131 CrossRef Medline
55. Miyazaki, K. (2011) MEGAWHOP cloning: a method of creating random mutagenesis libraries via megaprimer PCR of whole plasmids. *Methods Enzymol.* **498,** 399–406 CrossRef Medline
56. Peng, D., Kim, J. H., Kroncke, B. M., Law, C. L., Xia, Y., Droege, K. D., Van Horn, W. D., Vanoye, C. G., and Sanders, C. R. (2014) Purification and structural study of the voltage-sensor domain of the human KCNQ1 potassium ion channel. *Biochemistry* **53,** 2032–2042 CrossRef Medline
57. Delaglio, F., Grzesiek, S., Vuister, G. W., Zhu, G., Pfeifer, J., and Bax, A. (1995) NMRPipe: a multidimensional spectral processing system based on UNIX Pipes. *J. Biomol. NMR* **6,** 277–293 Medline
58. Vranken, W. F., Boucher, W., Stevens, T. J., Fogh, R. H., Pajon, A., Llinas, P., Ulrich, E. L., Markley, J. L., Ionides, J., and Laue, E. D. (2005) The CCPN data model for NMR spectroscopy: development of a software pipeline. *Proteins Struct. Funct. Bioinf.* **59,** 687–696 CrossRef